Biosensors and Bioelectronics 279 (2025) 117410

Contents lists available at ScienceDirect

Biosensors and Bioelectronics

journal homepage: www.elsevier.com/locate/bios

High-efficiency detection of APE1 using a defective PAM-driven CRISPR-Cas12a self-catalytic biosensor

Yang Song [a,1], Juan Long [b,1], Huaibi Wang [a], Wanyan Tang [a], Wei Yang [a], Yu Zheng [a], Rui Yuan [a], Decai Zhang [c,d,*], Bing Gu [d,**], Weiqi Nian [a,***]

[a] Department of Oncology, Chongqing Hospital of Traditional Chinese Medicine, Chongqing, 400016, China
[b] Chongqing Clinical Research Center for Dermatology, Chongqing Key Laboratory of Integrative Dermatology Research, Department of Dermatology, Chongqing Hospital of Traditional Chinese Medicine, Chongqing, 400016, China
[c] Department of Clinical Laboratory, The Fifth Affiliated Hospital, Sun Yat-sen University, Zhuhai, 519000, China
[d] Laboratory Medicine, Guangdong Provincial People's Hospital (Guangdong Academy of Medical Sciences), Southern Medical University, Guangzhou, 510000, China

ARTICLE INFO

Keywords:
CRISPR-Cas12a
Defective PAM
Self-catalytic signal amplification
APE1 detection
Point-of-care testing (POCT)

ABSTRACT

The trans-cleavage activity of the CRISPR-Cas system offers tremendous potential for developing highly sensitive and selective molecular diagnostic tools. However, conventional methods often face challenges such as limited catalytic efficiency of single Cas proteins and the necessity of complex multi-enzyme preamplification steps. To address these limitations, we present a novel defective PAM-mediated CRISPR-Cas12a self-catalytic signal amplification strategy, termed DEP-Cas-APE, for the rapid, sensitive, and specific detection of apurinic/apyrimidinic endonuclease 1 (APE1) activity. This approach integrates defective PAM-modified DNA probes to synergize Cas12a trans-cleavage with self-catalytic circuit, achieving efficient signal transformation and amplification under isothermal, one-step conditions. We systematically investigated the influence of defective PAM sequences containing apurinic/apyrimidinic (AP) sites on Cas12a activation and validated the feasibility of the DEP-Cas-APE strategy in detecting APE1. Under optimized conditions, DEP-Cas-APE achieved a detection limit as low as 7.66×10^{-8} U μL^{-1} within 30 min using a simple isothermal reaction. Additionally, we developed a point-of-care testing (POCT) platform by integrating DEP-Cas-APE with a colorimetric assay based on gold nanoparticles (AuNPs), enabling portable, equipment-free detection. This sensitive and selective strategy successfully detected APE1 in complex biological samples, including serum from lung cancer patients, and demonstrated the ability to distinguish cancerous from normal samples. DEP-Cas-APE represents a robust and versatile platform for advancing CRISPR-Cas12a biosensing technologies, offering new opportunities for molecular diagnostics and clinical research.

1. Introduction

The CRISPR-Cas system has revolutionized biotechnology, transforming molecular diagnostics beyond gene editing due to its simplicity, speed, efficiency, and cost-effectiveness (Zhu et al., 2020; Chertow, 2018; Broto et al., 2022). Among the various CRISPR systems, Cas12a (also known as Cpf1), a type V-A class 2 effector, has gained particular attention due to its unique capability of DNA-triggered trans-cleavage activity (Gayet et al., 2020; Shi et al., 2023). Over recent years, Cas12a has been extensively utilized to develop rapid, sensitive, and user-friendly biosensing platforms for detecting diverse biomolecules, including nucleic acids, small molecules, and protein biomarkers (Luo et al., 2022; Cui et al., 2023; Ding et al., 2024; Hu et al., 2024; Abnous et al., 2022; Wang et al., 2025). Despite these advances, most Cas12a-based assays still rely on preamplification steps, such as polymerase chain reaction (PCR) or isothermal amplification techniques, to achieve the sensitivity required for many applications (Li et al., 2018b; Chen et al., 2018; Wang et al., 2020). While such preamplification steps

* Corresponding author. Department of Clinical Laboratory, The Fifth Affiliated Hospital, Sun Yat-sen University, Zhuhai, 519000, China.
** Corresponding author.
*** Corresponding author.
E-mail addresses: zhangdecai2000@163.com (D. Zhang), gubing@gdph.org.cn (B. Gu), nwqone@126.com (W. Nian).
[1] These authors contributed equally to this work.

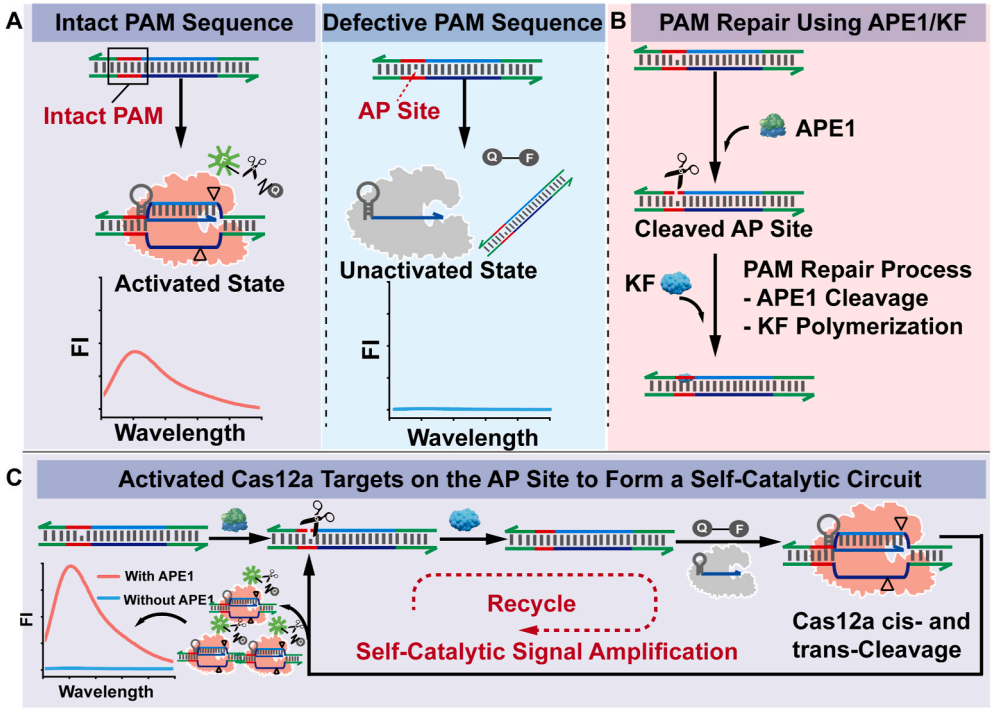
https://doi.org/10.1016/j.bios.2025.117410
Received 23 December 2024; Received in revised form 7 March 2025; Accepted 24 March 2025
Available online 24 March 2025
0956-5663/© 2025 Published by Elsevier B.V.

improve sensitivity and specificity, they also increase the risk of aerosol contamination and complicate workflows. In contrast, self-catalytic strategies offer a more efficient alternative by surpassing the conventional one-to-one (1:1) binding interaction between the target molecule and Cas protein, thereby enabling enhanced signal conversion (Li et al., 2018a; Wu et al., 2021). Integrating self-catalytic systems into CRISPR-Cas12a-based assays thus represents a promising avenue for significantly improving sensing performance.

Self-catalytic systems, particularly those based on nucleic acid nanotechnology, have found widespread applications in biosensing. Techniques such as hybridization chain reaction (HCR) (Qiao et al., 2023; Kachwala et al., 2021) and catalytic hairpin assembly (CHA) (Pan et al., 2023) facilitate the detection of inputs and the generation of amplified outputs through cascade or cyclic reactions under isothermal conditions. When integrated with CRISPR-Cas systems, these modular self-catalytic strategies can convert target information into substrate double-stranded DNA (dsDNA) for precise cleavage. However, in most implementations, Cas proteins are predominantly employed for endpoint analyses, leaving their broader potential for simultaneous identification and cleavage underutilized (Lv et al., 2021; Liu et al., 2022). Additionally, activated Cas12a can suffer from nonspecific degradation of template DNA within DNA circuits, resulting in unwanted interactions and signal leakage, which can compromise the stability and reliability of the assay. Thus, there remains a critical need for a fully integrated, efficient, and rapid CRISPR-Cas self-catalytic feedback system to overcome these limitations and enhance the performance of molecular diagnostics.

The Cas12a protein exhibits unique DNA cis-recognition and non-specific single-stranded DNA (ssDNA) trans-cleavage capabilities, positioning it as a transformative tool in molecular diagnostics. Previous studies have shown that Cas12a specifically recognizes and binds to the protospacer adjacent motif (PAM) on the target double-stranded DNA (dsDNA) via its PAM-interacting domain (Zetsche et al., 2015; Swarts et al., 2017; Swarts and Jinek, 2019; Stella et al., 2017). This interaction is mediated by hydrogen bonds and van der Waals forces between the PAM sequence and Cas12a, initiating unwinding activity that destabilizes the target DNA and facilitates strand separation. Following this, the CRISPR RNA (crRNA) hybridizes with the metastable target strand (TS), forming a critical R-loop structure necessary for Cas12a-mediated cis- and trans-cleavage activity. Despite these advances, the composition and functional properties of PAM sequences, along with their regulatory role in modulating Cas12a activation, remain inadequately studied. Further exploration of these aspects is crucial for optimizing Cas12a-based molecular diagnostics and expanding its applications.

In this study, we systematically explored the impact of base deletion within the PAM sequence on the activation efficiency of the Cas12a protein. We then proposed a novel defective PAM-mediated CRISPR-Cas12a self-catalytic signal magnifier for the rapid, specific, and sensitive detection of apurinic/apyrimidinic endonuclease 1 (APE1) activity, which we termed DEP-Cas-APE. This innovative approach involves the incorporation of an apurinic/apyrimidinic (AP) site within the PAM sequence of a double-stranded DNA (dsDNA) activator. As illustrated in Scheme 1A, the introduction of an AP site into the PAM sequence disrupts Cas12a recognition, keeping the nuclease activity in an inactive state. Conversely, dsDNA with an intact PAM sequence efficiently activates Cas12a, triggering trans-cleavage activity and leading to the cleavage of fluorescent probes. In Scheme 1B, we show that APE1 specifically cleaves the AP site, followed by Klenow Fragment (KF) DNA polymerase-mediated repair of the PAM sequence, which subsequently activates Cas12a's nuclease activity. The trans-cleavage activity of Cas12a on AP sites further promotes the disruption of the traditional 1:1 binding mode, enabling efficient signal transformation and amplification (Scheme 1C and Fig. S1). With its stringent cis recognition and efficient trans-cleavage activity, alongside carefully designed self-catalyzing DNA probes, DEP-Cas-APE ensures both high sensitivity and specificity in detection. We demonstrated the utility of the DEP-Cas-APE strategy in detecting the tumor marker APE1 (Song et al., 2021; Zhang et al., 2016; Wei et al., 2017; Pascut et al., 2019; Xie et al., 2019; Lee et al., 2020), showing excellent selectivity and high sensitivity for tumor marker signal amplification. Additionally, we developed a homogeneous colorimetric analysis platform based on gold nanoparticles (AuNPs), facilitating portable, efficient, and field-deployable analyte detection (POCT). Therefore, DEP-Cas-APE not only offers a new



Scheme 1. Schematic Illustration of the DEP-Cas-APE Platform for Detecting APE1 Activity.

approach for designing CRISPR-Cas12a-based biosensing systems but also establishes versatile signal output platforms, enhancing the robustness and practicality of detection systems in real-world applications.

2. Materials and methods

Details about the required materials, reagents, instruments and the methods for the supplementary experiments are provided in the Supporting Information.

2.1. Fluorescence measurement of DEP-Cas-APE

First, the model target dsDNA probes (MP) were denatured at a 1:1.2 ratio of TS to NTS in 1 × NEBuffer 3.0 by heating at 90 °C for 10 min, followed by annealing at 37 °C for 1h. Afterwards, APE1 at varying concentrations was added into a 100 μL reaction mixture containing 1 μL of 0.8 μM MP, 10 μL of 10 × NEBuffer 3.0, 5×10^{-2} U μL^{-1} of KF, 1 μL of 25 mM dNTP, 40 U μL^{-1} of RNase inhibitor, 1 μL of 2 μM Cas12a, 1 μL of 1 μM crRNA, and 1 μL of 50 μM FQ-ssDNA. The mixture was then incubated at 37 °C for 30 min. After incubation, fluorescence signals were measured using an FS5 fluorescence spectrophotometer.

2.2. Preparation of DNA-AuNPs

Initially, 88.2 mL of 1 mM $HAuCl_4$ solution was added to a round-bottom flask, heated, and stirred. After boiling, 10.1 mL of 34 mM sodium citrate solution was quickly added, and the mixture was allowed to continue boiling for 10 min. The heating was then stopped, but stirring continued for another 15 min before cooling to room temperature. The resulting AuNPs solution appeared wine red with an approximate diameter of 13 nm and was stored at 4 °C in the dark (Grabar et al., 1995; Siti et al., 2012). The functionalization of AuNPs and the conjugated DNA probes (Table S3) is based on the methodology described by Ma et al. (2022). Firstly, 2 μL of 500 nM TCEP was added to 8 μL of 100 μM DNA 1 and DNA 2 respectively, and the mixture was left at room temperature for 30 min. After mixing with 200 μL of AuNPs and freezing at −20 °C for 2 h, the coupling of DNA-AuNPs was completed. The mixture was then thawed at room temperature, centrifuged at 12,000 rpm for 30 min, the supernatant was removed, and the pellet was washed three times with 5 mM HEPES buffer (pH 7.6). Finally, DNA-AuNPs were resuspended in 10 mM HEPES buffer containing 300 mM NaCl (pH 7.6) and stored at 4 °C in the dark. UV–vis absorbance at 520 nm was measured using a UV–vis spectrophotometer.

2.3. Colorimetric measurement of DEP-Cas-APE

The target APE1 at different concentrations was added to a 70 μL mixture containing 1 μL of 0.8 μM MP, 7 μL of 10 × NEBuffer 3.0, 5×10^{-2} U μL^{-1} of KF, 1 μL of 25 mM dNTP, 40 U μL^{-1} of RNase inhibitor, 1 μL of 2 μM Cas12a, 1 μL of 1 μM crRNA, and 1 μL of 2 μM Linker ssDNA. The mixture was then incubated at 37 °C for 30 min. Cas12a was induced to trans-cleave the Linker ssDNA and then inactivated at 65 °C for 5 min. Subsequently, 15 μL of DNA-AuNPs1 and DNA-AuNPs2 were added and incubated at 37 °C for 6 min to facilitate the coupling aggregation of DNA-AuNPs with Linker ssDNA. The colorimetric image of the solution was captured using a smartphone, and the absorption intensity at 520 nm was measured using a UV–Vis spectrophotometer.

2.4. Dynamics analysis

The probe was modified at the 5′ end of TS2-2 (TS2-2*) and the 3′ end of NTS2 (NTS2*) with a pair of dye/quencher agents (FAM/BHQ1). The TS2-2* and NTS2* strands were denatured in 1 × NEBuffer 3.0 at 90 °C for 10 min at a ratio of 1:1.2, and then annealed at 37 °C for 1 h to generate model report probes (Table S1). To study the catalytic kinetics of APE1 and Cas12a, 1×10^{-2} U μL^{-1} of APE1 was added to a 100 μL reaction mixture. This mixture consisted of 1 μL of 50 μM model report probes, 10 μL of 10 × NEBuffer 3.0, 5×10^{-2} U μL^{-1} of KF, 1 μL of 25 mM dNTP, 40 U μL^{-1} of RNase inhibitor, 1 μL of 2 μM Cas12a, and 1 μL of 1 μM crRNA. RNase-free water was added to adjust the final volume to 100 μL. The blank control did not contain APE1. For APE1 activity analysis, 1×10^{-2} U μL^{-1} of APE1 was introduced into a 100 μL mixture containing 1 μL of 50 μM model report probes, 10 μL of 10 × NEBuffer 3.0, 5×10^{-2} U μL^{-1} of KF, 1 μL of 25 mM dNTP and 40 U μL^{-1} of RNase inhibitor. RNase-free water was used to ensure the total volume reached 100 μL. The above mixtures were incubated at 37 °C. The fluorescence intensity was monitored every 100 s for 30 min using an FS5 fluorescence spectrophotometer.

2.5. Extraction of nucleus proteins

Cells were harvested after reaching 80 % confluency in a cultured dish. All cells were washed twice with 1 × Sterile PBS and treated with 1 mL trypsin at 37 °C for 2 min. After treatment, an equal amount of DMEM was added to the isolated cells to inactivate the trypsin. The cell mixtures were then collected into sterile centrifuge tubes and harvested by centrifugation at 1000 rpm for 5 min. After centrifugation, the supernatant was discarded, and 1 mL of fresh 1 × Sterile PBS was added for cell counting using a Beckman cell counter. The cell pellet was subsequently obtained by centrifugation again. Ice-cold Cytoplasmic Extraction Reagent I (CER I) was added to the cell pellet and incubated for 10 min. Cytoplasmic Extraction Reagent II (CER II) was then added to the mixture and incubated for 1 min. The cell lysates were centrifuged at 3500 rpm, and the pellet was resuspended in Nuclear Extraction Reagent (NER) for 40 min on ice. Finally, the supernatants containing the nuclear proteins were collected by centrifugation at 14,000 rpm. The obtained proteins were stored at −80 °C for future use.

2.6. Clinical sample analysis

Serum samples from lung cancer patients and healthy individuals were collected from Chongqing Hospital of Traditional Chinese Medicine, with approval from the hospital's medical ethics committee in accordance with the Helsinki Declaration. Initially, the serum samples were centrifuged at 1000 g for 10 min at 37 °C. After centrifugation, APE1 levels were detected using the one-step DEP-Cas-APE assay, following the procedures described above.

3. Results and discussion

3.1. Influence of PAM with AP site on Cas12a activation

The presence of the PAM sequence is essential for Cas12a to recognize and bind to target DNA, highlighting the importance of maintaining PAM integrity for accurate target region identification (Chen et al., 2018). We hypothesize that the absence of bases in the PAM or its complementary sequence could interfere with Cas12a′s ability to accurately recognize the target dsDNA, significantly affecting its nuclease activity (Fig. 1A and B). To test this hypothesis, MP were designed with an AP site positioned within the PAM or its complementary sequence to evaluate their impact on Cas12a′s nuclease activity (Fig. 1C and F). For comparison, APE1 was employed to excise the AP site, followed by repair of the cleavage site by DNA polymerase, generating intact target dsDNA for Cas12a activation. It was observed that introducing an AP site into the 5′-TTTC-3′ PAM sequence and its complementary sequence had minimal effect on Cas12a′s trans-cleavage activity (Fig. 1D and G). However, inserting an AP site into the 5′-TTC-3′ PAM sequence and its complementary sequence led to a significant reduction in the fluorescent signal. Notably, when the AP site was positioned between T and C in the 5′-TTC-3′ PAM sequence, there was a significant inhibition of Cas12a′s nuclease activity, with an F/F_0 value of 32.3 (Fig. 1E), where F

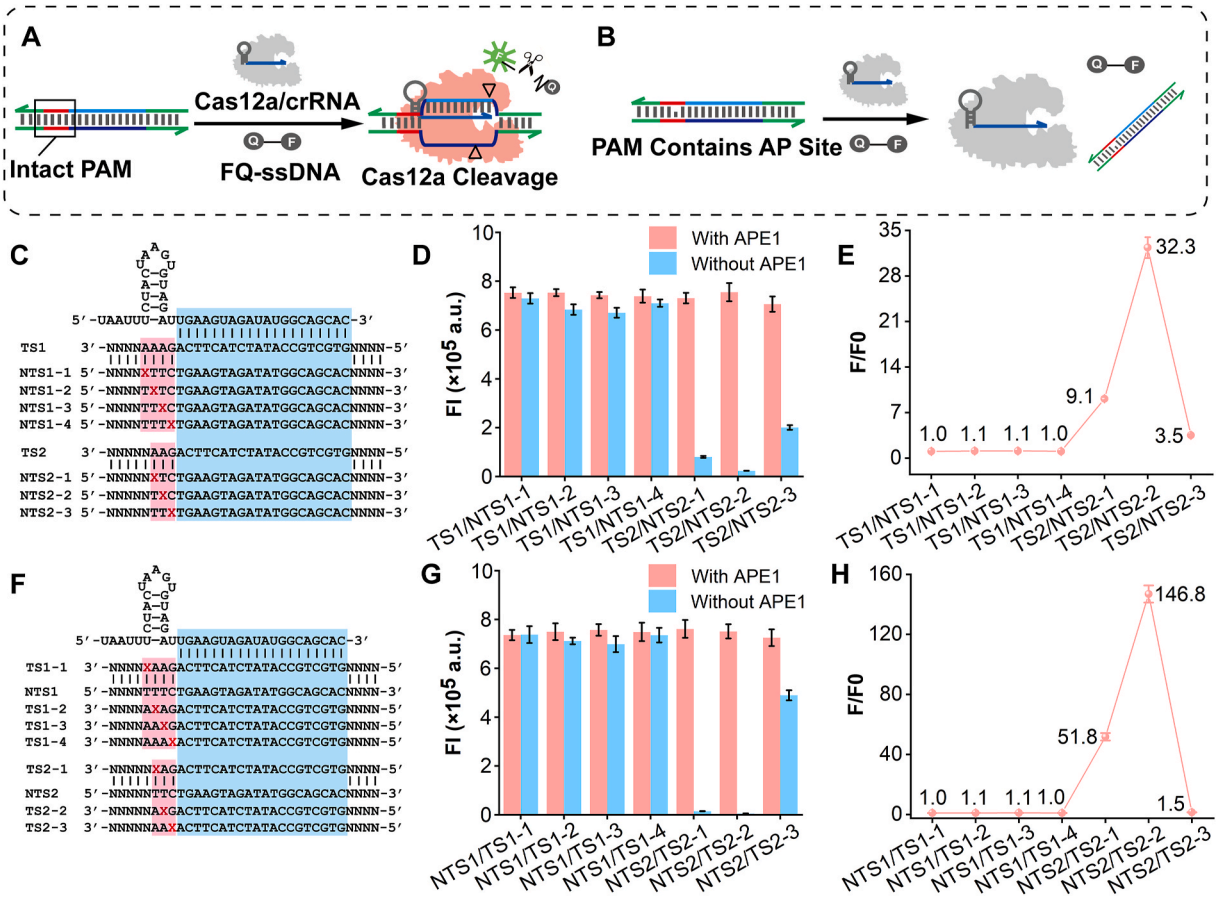


Fig. 1. Cas12a activation affected by AP site within the PAM sequence. (A and B) Schematic illustration of Cas12a recognition of the classical PAM and PAM containing AP sites. (C) Positions of AP sites within the PAM sequence. (D) Fluorescence intensity and (E) F/F0 values for AP site-modified PAM, with or without APE1. (F) Positions of AP sites within the PAM complementary sequence. (G) Fluorescence intensity and (H) F/F0 values for AP site-modified PAM complementary sequence, with or without APE1.The concentration of target dsDNA was 0.8 μM. λex: 490 nm, λem: 520 nm.

represents the fluorescence intensity observed in the presence of APE1, while F_0 denotes the fluorescence intensity without APE1. In contrast, when the AP site was positioned between A and G in the complementary sequence of PAM, there was almost complete inhibition of Cas12a′s nuclease activity, with an F/F_0 value of approximately 150 (Fig. 1H). A possible reason is that Cas12a is unable to recognize the T-rich sequence in double-stranded DNA, and the extra base at the 5′ terminal of NTS-b is more effective in blocking the spacer domain. This dual effect ensures that Cas12a remains in an inactive state, leading to stronger inhibition. This result is consistent with our previous findings (Zhang et al., 2022). Interestingly, a similar phenomenon was observed when the corresponding sequence location was deleted, leading to the formation of nicked dsDNA, which also inhibited Cas12a activation (Fig. S2). These results suggest that a PAM sequence consisting of at least two thymine (T) bases is critical for activating the Cas12a protein. Additionally, the complementarity of the two T-base PAM sequences is indispensable, especially the base located on the complementary strand, which plays a more critical role in activating Cas12a. However, PAM sequences with three T bases showed greater tolerance to incomplete complementation. Additionally, the results clearly demonstrate that in the presence of APE1, when the AP site is cleaved and the complementary sequence of PAM is repaired by DNA polymerase, MP is converted into a functional activator recognized by Cas12a, thereby restoring its trans-cleavage activity.

3.2. Feasibility of the DEP-Cas-APE strategy

To validate the feasibility of the DEP-Cas-APE biosensing strategy, we first used MP containing an AP site, which were formed by hybridizing TS2-2 and NTS2, as described previously. A series of fluorescence experiments were then conducted using 5′-FAM and 3′-BHQ-labeled ssDNA (ssDNA-FQ) as the substrate for Cas12a trans-cleavage. The presence of APE1 resulted in a significant enhancement of the fluorescence response, as shown in Fig. 2A, indicating effective cleavage of the ssDNA-FQ reporter and subsequent restoration of the fluorescence signal. In contrast, without APE1, the fluorescence response was nearly undetectable. Moreover, fluorescence signals were negligible in the absence of MP, KF, crRNA, or Cas12a protein. These results confirm the successful establishment of the DEP-Cas-APE strategy and highlight the essential roles of MP, crRNA, Cas12a protein, and KF in the system.

To further validate these fluorescence results, we performed 12 % polyacrylamide gel electrophoresis (PAGE). As shown in Fig. 2B, the hybridization of TS2-2 (lane 1) and NTS2 (lane 2) resulted in the formation of MP (lane 3). Under the catalytic action of APE1, the AP site in the PAM complementary sequence of MP was cleaved, followed by extension and strand displacement reactions mediated by KF, producing a distinct band approximately 17 bases in length (lane 4). This confirms the role of DNA polymerase in preserving the integrity of the PAM complementary sequence, converting MP into a dsDNA activator that is recognizable by Cas12a. Consequently, the activated Cas12a nuclease effectively cleaved both of the dsDNA activator and a 20-nucleotide ssDNA (lanes 6 and 7). Conversely, in the absence of APE1, Cas12a nuclease activity was not induced (lanes 8). These findings collectively validate the feasibility of using the DEP-Cas-APE strategy for APE1 detection.

Based on these results, we hypothesize that the trans-cleavage

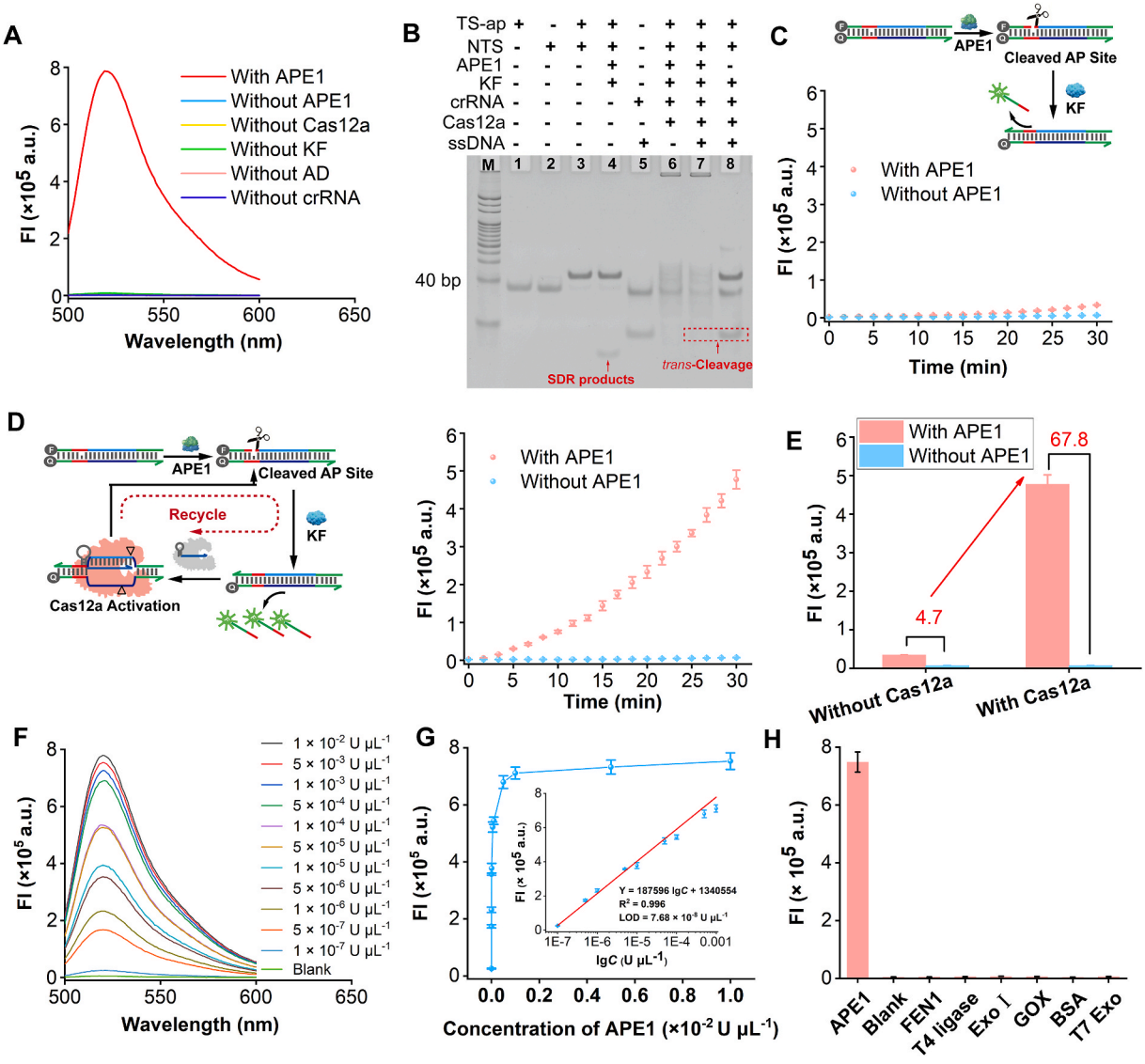


Fig. 2. Feasibility and performance of the DEP-Cas-APE for APE1 detection. (A) Fluorescence spectra of the DEP-Cas-APE system obtained from different samples. (B) 12 % PAGE analysis: Lane 1, TS; Lane 2, NTS; Lane 3, TS + NTS; Lane 4, TS + NTS + APE1 + KF; Lane 5, crRNA + ssDNA; Lane 6, APE1 + TS + NTS + KF + crRNA + Cas12a; Lane 7, APE1 + TS + NTS + KF + crRNA + Cas12a + ssDNA; Lane 8, TS + NTS + KF + crRNA + Cas12a + ssDNA. (C) Real-time fluorescence monitoring curves in the absence of Cas12a/crRNA. (D) Real-time fluorescence monitoring curves in the presence of Cas12a/crRNA. (E) Signal-to-background ratio analysis for end-point fluorescence detection. (F) Fluorescence spectra responding to APE1 at varying concentrations. (G) Linear relationship between fluorescence intensity and APE1 concentrations, ranging from 1.0×10^{-7} U μL^{-1} to 1.0×10^{-3} U μL^{-1}. (H) Comparative fluorescence intensities of APE1 and other protein species.

activity of Cas12a not only induces non-specific cleavage of ssDNA but also efficiently targets and cleaves the AP site, thereby initiating a self-catalytic amplification process. As illustrated in Fig. 2C, we modified the 5′ end of the TS2-2 strand and the 3′ end of the NTS2 strand with fluorescence (FAM) and quencher (BHQ1) groups, respectively, forming a double-stranded signal probe upon hybridization. In the direct detection assay, APE1 cleaves the AP site, triggering a polymerase-mediated extension reaction that replaces the excised TS2-2 segment. This disrupts the fluorescence resonance energy transfer (FRET) between FAM and BHQ1, generating a fluorescence signal. When co-incubated with Cas12a/crRNA, the signal probe is converted into a double-stranded DNA trigger, activating Cas12a′s trans-cleavage activity. This, in turn, targets the AP site, continuously initiating the PAM repair process in the presence of KF, leading to repeated activation of Cas12a and progressive replacement of additional TS2-2 segments, ultimately resulting in significant fluorescence enhancement (Fig. 2D). As shown in Fig. 2E, the signal-to-background (S/B) ratio increased from 4.7 to 67.8, demonstrating the effectiveness of Cas12a-mediated self-catalytic amplification in signal enhancement.

To further validate this amplification effect, we conducted additional experiments comparing the three different detection modes for APE1 at varying concentrations. As shown in Fig. S3, the results demonstrated that Cas12a-mediated self-catalytic amplification improved sensitivity by at least three orders of magnitude compared to direct detection. Furthermore, the introduction of the ssDNA-FQ probe significantly enhanced the signal, as the activated Cas12a trans-cleaved the probe, establishing the DEP-Cas-APE system and further improving detection sensitivity. These findings collectively confirm the successful implementation of Cas12a-mediated self-catalytic amplification, underscoring its remarkable ability to enhance detection sensitivity and establish it as a highly effective tool for ultra-sensitive APE1 detection.

3.3. *Performance of the DEP-Cas-APE strategy*

Under the optimized experimental conditions (Fig. S4), the analytical performance of the DEP-Cas-APE biosensing method was evaluated

by measuring various concentrations of APE1. As shown in Fig. 2F, the fluorescence signal increases proportionally with APE1 concentrations ranging from 1.0×10^{-7} U μL^{-1} to 1.0×10^{-3} U μL^{-1}. Within this range, the fluorescence intensity at 520 nm exhibited a strong linear correlation with the logarithm of APE1 concentration, with the regression equation $Y = 187596\ \lg C + 1340554$ ($R^2 = 0.996$), where Y represents the fluorescence intensity and C denotes the concentration of APE1 (Fig. 2G). The limit of detection (LOD), calculated as the mean of the blank sample plus three times the standard deviation, was found to be 7.68×10^{-8} U μL^{-1}. This demonstrates enhanced sensitivity compared to previous studies (Table S5). The high efficiency and sensitivity of the biosensor are primarily attributed to two key factors: (i) the incorporation of AP sites into the PAM complementary sequence in the dsDNA trigger, which effectively regulates Cas12a activity, significantly reducing background signals and improving S/B ratios; (ii) the activated Cas12a-catalyzed enzymatic reaction, which synergistically interacts with the AP sites to establish a self-catalysis for signal amplification. This process accelerates the reaction kinetics, improves overall efficiency, and results in dual amplification of the target signal.

To assess the specificity of the biosensor, experiments were conducted with several potential interfering proteins, including FEN1, T4 ligase, Exo I, GOX, BSA, and T7 Exo. As shown in Fig. 2H, the target APE1 produced a strong fluorescence signal, while unrelated proteins and the blank control resulted in only weak signals near background levels. This demonstrates negligible cross-talk or interference, confirming high selectivity of the method for APE1 detection. Additionally, to assess the reproducibility of the biosensor, five parallel measurements of APE1 at a concentration of 0.001 U μL^{-1} were performed. The results showed a low relative standard deviation (RSD <5 %), indicating excellent reproducibility.

3.4. Application evaluation of the proposed strategy

To evaluate the potential of the proposed strategy in complex biological samples, the standard addition technique was applied by introducing varying concentrations of APE1 into buffer solutions and diluted serum from healthy individuals. As shown in Fig. 3A, the fluorescence intensities of target APE1 in both buffer and diluted human serum were comparable. The recovery rates ranged from 96.07 % to 105.14 %, with RSD between 7.45 % and 9.34 % (Supplementary Table S4). These

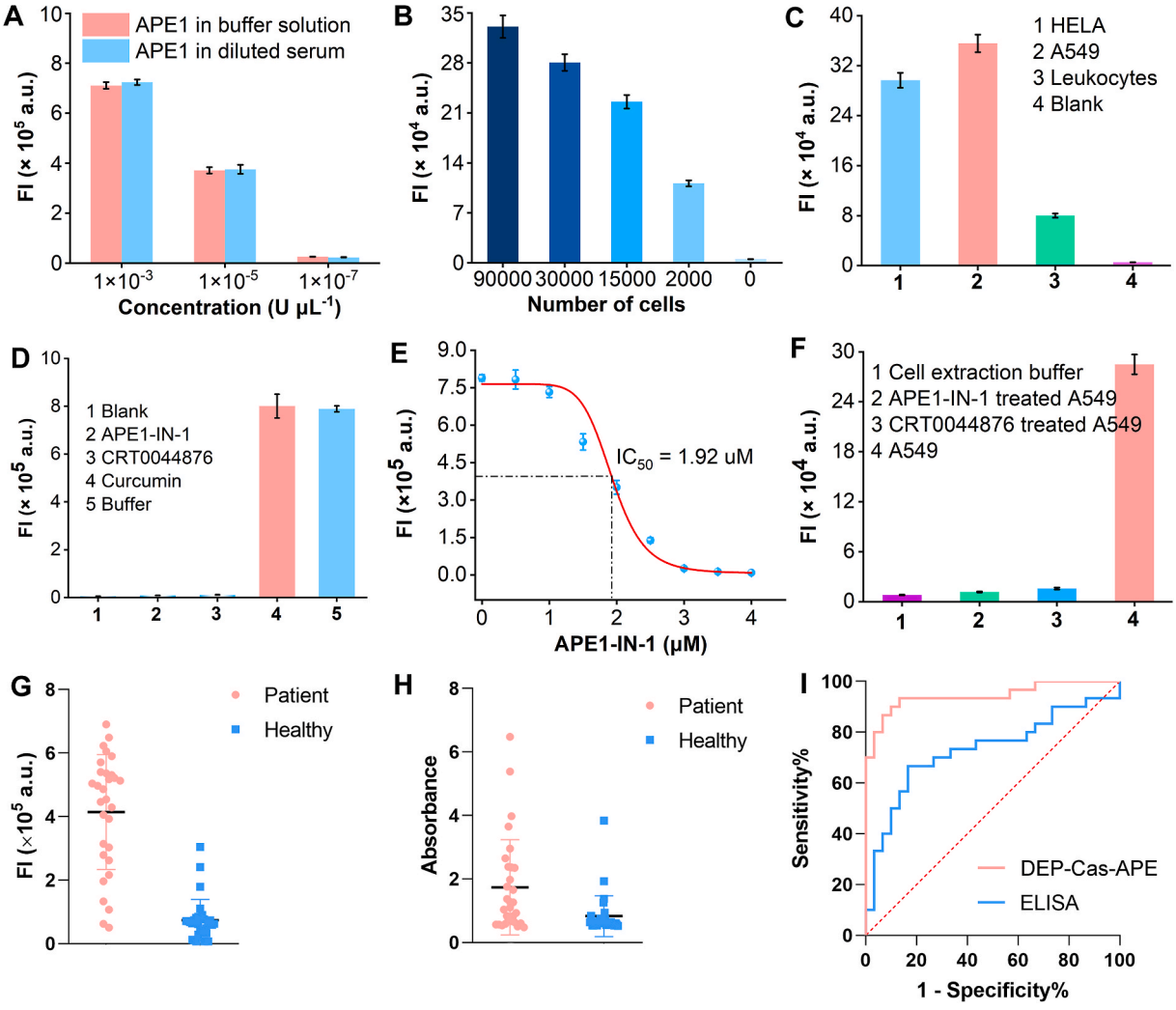


Fig. 3. Application of the DEP-Cas-APE strategy. (A) Comparison of fluorescence intensities between diluted serum and buffer. (B) Fluorescence intensity of the APE1 detection system in response to lysates from varying numbers of HeLa cells. (C) Fluorescence intensity of the APE1 detection system in response to lysates from different human cells, with the same number of cells (30000). (D) Evaluation of the inhibitory effects of different chemical substances on APE1 activity. (E) Changes in APE1 relative activity with increasing concentrations of APE1-IN-1. (F) Fluorescence signal response of APE1 activity in extracts from HeLa and A549 cells, and the inhibitory effects of APE1 inhibitors APE1-IN-1 and CRT0044876 on APE1 activity in A549 cell extracts. (G) and (H) Box plots showing the APE1 activity detection in serum samples from 30 healthy donors (blue) and 30 lung cancer patients (pink) using the DEP-Cas-APE strategy and the commercial APE1 ELISA kit. (I) ROC curves comparing the diagnostic performance of the DEP-Cas-APE strategy and the commercial APE1 ELISA kit in clinical serum samples.

results confirm that serum has a negligible effect on the performance of the biosensor.

To further investigate the practical application of this biosensor, fluorescence assays were conducted using different cell lines. As depicted in Fig. 3B, the fluorescence signals detected in lysates from 2000 HeLa cells were significantly higher than the blank background. A progressive increase in fluorescence signals was observed as cell numbers increased to 90000, demonstrating the method's ability to quantitatively determine APE1 levels in live cells. Furthermore, the biosensor was used to compare APE1 expression levels in different human cells. As shown in Fig. 3C, the fluorescence signals in lysates from human lung adenocarcinoma cells (A549) and HeLa cells were significantly higher than those in MCF-10A (normal epithelial cells) lysates and clearly exceeded the blank background. To validate these findings, we compared APE1 levels using a commercially available enzyme-linked immunosorbent assay (ELISA) kit (Fig. S5). The results revealed significant differences in APE1 expression between normal and cancer cells, consistent with prior studies (Xu et al., 2021; Yi et al., 2021). These findings highlight the elevated APE1 levels in cancer cells compared to normal cells, supporting the proposed method's potential for precise discrimination in clinical diagnostics.

Recent studies have indicated that inhibiting APE1 activity could impede cancer progression, making it a promising target for the development of anticancer therapeutics. To investigate this, we performed inhibition experiments using APE1-IN-1 and CRT0044876 as positive controls, with curcumin and buffer serving as negative controls. As shown in Fig. 3D, fluorescence signals were markedly reduced in the presence of inhibitors, confirming the effective suppression of APE1 activity by APE1-IN-1 and CRT0044876. Additionally, a concentration-dependent decrease in APE1 activity was observed when incubated with increasing concentrations of APE1-IN-1 (Fig. 3E), yielding an IC50 value of 1.92 μM. Moreover, fluorescence intensities of cell lysates treated with APE1-IN-1 and CRT0044876 were significantly lower compared to untreated samples (Fig. 3F). These results demonstrate the feasibility of the proposed strategy for screening APE1 inhibitors and highlight its potential as a robust platform for both cancer diagnostics and drug discovery.

3.5. Measurement of APE1 activity in clinical specimens from lung cancer patients

Lung cancer is one of the most prevalent malignancies, and numerous studies have highlighted a strong correlation between APE1 and the progression of lung cancer. To evaluate the feasibility of our strategy for clinical diagnostics, we collected a total of 60 serum samples, including 30 from healthy individuals and 30 from biopsy-confirmed lung cancer patients. The performance of our novel DEP-Cas-APE strategy in diagnosing lung cancer was compared to that of commercially available ELISA kits. As shown in Fig. 3G and H, APE1 expression levels in serum samples from lung cancer patients were significantly higher than those in healthy individuals, consistent with the results obtained using the ELISA method. Furthermore, receiver operating characteristic (ROC) curves were used to assess the diagnostic accuracy of different methods. As depicted in Fig. 3I, the area under the curve (AUC) for the DEP-Cas-APE strategy was 0.94, significantly outperforming the traditional ELISA method, which had an AUC of 0.73. The optimal cut-off value was 2.4×10^{-7} U μL^{-1}, resulting in 93.3 % sensitivity and 86.7 % specificity. Since the LOD is significantly lower than the cutoff value, our sensor possesses sufficient sensitivity to detect APE1 concentrations relevant to lung cancer diagnosis, demonstrating the superiority of our diagnostic strategy over ELISA by offering a more streamlined and convenient approach for APE1 detection.

3.6. Application of colorimetric analysis

The potential application of the developed method for POCT was explored by integrating it with an AuNPs colorimetric output platform (Zhao et al., 2008; Zagorovsky and Chan, 2013; Wang et al., 2021; Lee et al., 2024). As shown in Fig. S6A, the prepared DNA-AuNPs 1 and DNA-AuNPs 2 exhibited a burgundy color, indicating successful attachment of DNA probes to the surface of AuNPs and their homogeneous dispersion. In contrast, AuNPs without DNA probes displayed complete aggregation and precipitation when frozen. Additionally, the UV–vis absorption peak of both unfrozen AuNPs and DNA-AuNP probes exhibited a 4 nm redshift, further confirming successful DNA conjugation on the AuNP surface. Transmission electron microscopy (TEM) analysis revealed that the unfrozen AuNPs and DNA-AuNPs 1 displayed excellent dispersibility, whereas the frozen bare AuNPs were completely aggregated (Figs. S6B, C, and D). As shown in Fig. 4A, the degradation of the linker ssDNA, triggered by Cas12a activity in the presence of APE1, led to the dispersion of DNA-AuNPs, resulting in a vivid red solution with high absorbance, as confirmed by UV–vis spectroscopy. In contrast, in the absence of APE1, the defective PAM sequence hindered Cas12a/crRNA recognition of the dsDNA, preventing cleavage activation. As a result, linker ssDNA and DNA-AuNPs cross-linked, inducing aggregation of AuNPs, leading to a shift in the absorption peak and a lighter solution color.

The feasibility of Cas12a-mediated trans-cleavage regulation of AuNPs for colorimetric analysis was validated through visual inspection, UV–vis spectroscopy, and TEM. As shown in Fig. 4B, in the presence of APE1, DNA-AuNPs dispersed, forming a vivid red solution with strong UV–vis absorbance. Conversely, in the absence of APE1, AuNP aggregation occurred, leading to a reduction in UV–vis absorption intensity, a redshift in the absorption peak, and a lighter solution color. TEM analysis further revealed that the presence of APE1 induced a transition in the state of the gold nanoparticles from aggregation to dispersion, validating the method's feasibility (Fig. 4C). As depicted in Fig. 4D, the UV–vis absorbance at 520 nm increased with the concentration of APE1. A strong linear correlation was observed within the concentration range of 1.0×10^{-4} U μL^{-1} to 1.0×10^{-2} U μL^{-1}, with the regression equation: $Y = 0.096\ \lg C + 1.382$ ($R2 = 0.993$), where Y represents absorbance and C denotes the concentration of APE1 (Fig. 4E). The LOD was calculated to be 4.17×10^{-4} U μL^{-1}. Selectivity experiments indicated that colorimetric signal restoration occurred only in the presence of target APE1 (Fig. 4F). These results demonstrate that our strategy successfully integrates nanomaterial-based colorimetric sensing, highlighting its significant potential for POCT applications.

4. Conclusion

In summary, we conducted an in-depth investigation into the regulation of base deletion in PAM sequences and its impact on Cas12a protein activity. Based on the findings, we developed a novel strategy, termed DEP-Cas-APE, which leverages defective PAM-mediated CRISPR-Cas12a self-catalytic circuits for signal amplification, enabling efficient detection of APE1 activity. Our results demonstrate that Cas12a activity can be effectively regulated by incorporating an AP site into the complementary sequence of 5′-TTC-3′, which minimizes background signals and an improvs signal-to-noise ratio. The DEP-Cas-APE method is a straightforward, one-step process that can be completed in just 30 min under isothermal conditions. Moreover, this system is compatible with nanomaterial colorimetric sensing technology and does not require large-scale, precision equipment, making it highly suitable for POCT settings with limited resources. The DEP-Cas-APE provides a direct and efficient method for detecting even trace amounts of APE1, highlighting its significant potential in both biochemical and molecular biological research as well as clinical diagnostics. Despite these promising results, certain limitations remain and should be addressed in future iterations. First, implementing lyophilization could enhance assay stability by extending reagent shelf-life, which in turn facilitates long-term storage and transportation. Furthermore, optimizing DNA probe design and CRISPR-Cas12a recognition elements could broaden the DEP-Cas-APE

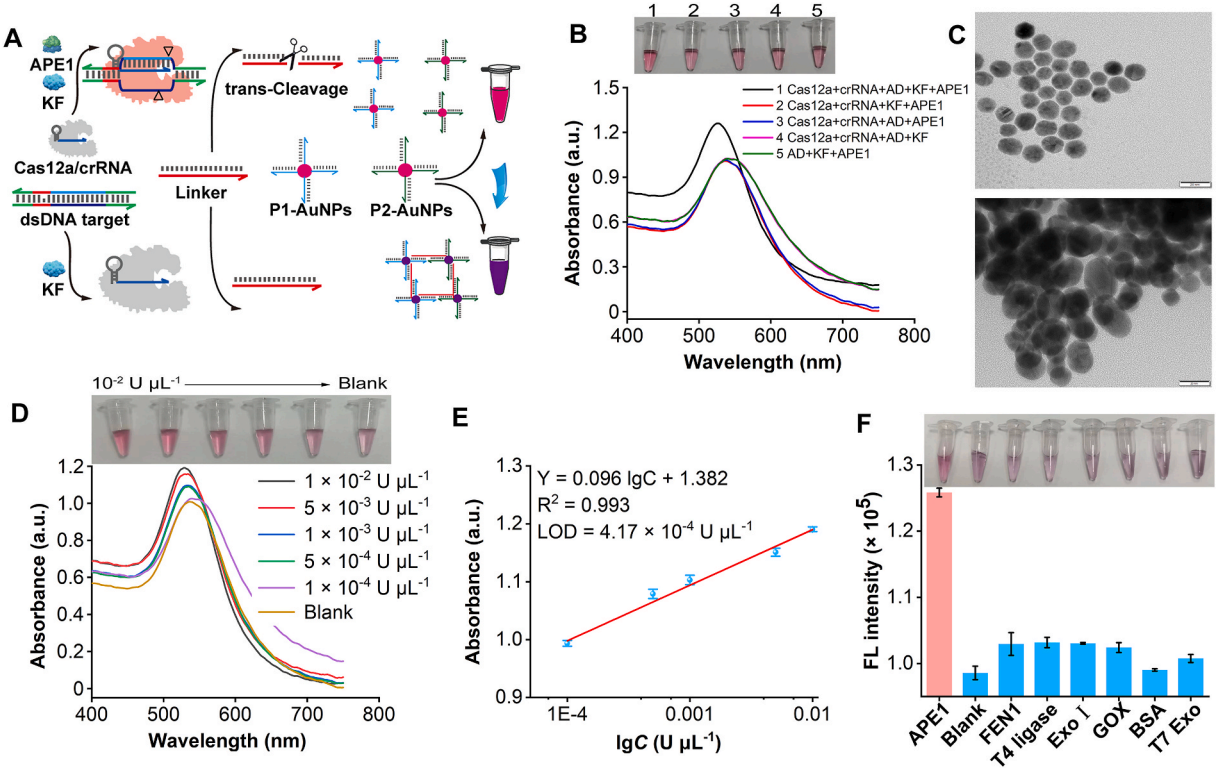


Fig. 4. (A) Schematic representation of the DEP-Cas-APE strategy integrated with AuNPs colorimetric output platform. (B) Photographs and UV spectra of AuNPs in the DEP-Cas-APE system obtained from different samples. (C) TEM images of tubes 1 and 5 (representing dispersed and aggregated AuNPs) from Fig. 4B. (D) Visual colorimetry and UV–vis spectra of APE1 reaction solutions at varying concentrations. (E) Linear relationship between UV–vis absorbance intensity and the logarithmic concentration of APE1, ranging from 1×10^{-4} to 1×10^{-2} U μL^{-1}. (F) UV–vis absorption intensity and visual colorimetry of other protein species compared to APE1.

system's applicability, thus enabling the detection of a wider range of targets beyond APE1. In addition, integrating the assay with a portable detection device, such as a smartphone-based biosensor, could support real-time, field-deployable diagnostics with quantitative analytical capabilities.

CRediT authorship contribution statement

Yang Song: Writing – original draft, Methodology, Formal analysis, Data curation, Conceptualization. **Juan Long:** Methodology, Investigation, Formal analysis, Data curation. **Huaibi Wang:** Software, Resources, Formal analysis. **Wanyan Tang:** Resources, Methodology, Investigation. **Wei Yang:** Validation, Resources, Methodology. **Yu Zheng:** Visualization, Validation, Software. **Rui Yuan:** Visualization, Resources, Methodology. **Decai Zhang:** Writing – review & editing, Validation, Software, Methodology, Funding acquisition. **Bing Gu:** Validation, Supervision, Project administration, Funding acquisition. **Weiqi Nian:** Validation, Supervision, Resources, Project administration, Conceptualization.

Declaration of competing interest

The authors declare that they have no known competing financial interests or personal relationships that could have appeared to influence the work reported in this paper.

Acknowledgements

This work was supported by the National Natural Science Foundation of China (82102505, 82402754), the China Postdoctoral Science Foundation (2023M740767, 2023MD744145), the Chongqing Medical Leading Talent Project (YXLJ202401), the Chongqing Medical Scientific Research Project (Joint Project of Chongqing Health Commission and Science and Technology Bureau) (2024QNXM024), and the First Batch of Key Disciplines on Public Health in Chongqing.

Appendix A. Supplementary data

Supplementary data to this article can be found online at https://doi.org/10.1016/j.bios.2025.117410.

Data availability

Data will be made available on request.

References

Abnous, K., Khakshour Abdolabadi, A., Ramezani, M., Alibolandi, M., Nameghi, M.A., Zavvar, T., Khoshbin, Z., Lavaee, P., Taghdisi, S.M., Danesh, N.M., 2022. A highly sensitive electrochemical aptasensor for cocaine detection based on CRISPR-Cas12a and terminal deoxynucleotidyl transferase as signal amplifiers. Talanta 241, 123276.

Broto, M., Kaminski, M.M., Adrianus, C., Kim, N., Greensmith, R., Dissanayake-Perera, S., Schubert, A.J., Tan, X., Kim, H., Dighe, A.S., Collins, J.J., Stevens, M.M., 2022. Nanozyme-catalysed CRISPR assay for preamplification-free detection of non-coding RNAs. Nat. Nanotechnol. 17 (10), 1120–1126.

Chen, J.S., Ma, E., Harrington, L.B., Da Costa, M., Tian, X., Palefsky, J.M., Doudna, J.A., 2018. CRISPR-Cas12a target binding unleashes indiscriminate single-stranded DNase activity. Science 360 (6387), 436–439.

Chertow, D.S., 2018. Next-generation diagnostics with CRISPR. Science 360 (6387), 381–382.

Cui, C., Lau, C.H., Chu, L.T., Kwong, H.K., Tin, C., Chen, T.H., 2023. Multimodal detection of flap endonuclease 1 activity through CRISPR/Cas12a trans-cleavage of single-strand DNA oligonucleotides. Biosens. Bioelectron. 220, 114859.

Ding, S., Yuan, Y., Dong, J., Du, F., Cui, X., Shi, Z., Tang, Z., 2024. Leveraging CRISPR/Cas12 signal amplifier to sensitive detection of apurinic/apyrimidinic endonuclease 1 and high-throughput inhibitor screening. Anal. Chim. Acta 1291, 342212.

Gayet, R.V., De Puig, H., English, M.A., Soenksen, L.R., Nguyen, P.Q., Mao, A.S., Angenent-Mari, N.M., Collins, J.J., 2020. Creating CRISPR-responsive smart materials for diagnostics and programmable cargo release. Nat. Protoc. 15 (9), 3030–3063.

Grabar, K.C., Freeman, R.G., Hommer, M.B., Natan, M.J., 1995. Preparation and characterization of Au colloid monolayers. Anal. Chem. 67 (4), 735–743.

Hu, X., Li, J., Li, Y.T., Zhang, Y., Xiao, M.M., Zhang, Z., Liu, Y., Zhang, Z.Y., Zhang, G.J., 2024. Plug-and-play smart transistor bio-chips implementing point-of-care diagnosis of AMI with modified CRISPR/Cas12a system. Biosens. Bioelectron. 246, 115909.

Kachwala, M.J., Smith, C.W., Nandu, N., Yigit, M.V., 2021. Reprogrammable gel electrophoresis detection assay using CRISPR-Cas12a and hybridization chain reaction. Anal. Chem. 93 (4), 1934–1938.

Lee, S., Dang, H., Moon, J.I., Kim, K., Joung, Y., Park, S., Yu, Q., Chen, J., Lu, M., Chen, L., Joo, S.W., Choo, J., 2024. SERS-based microdevices for use as in vitro diagnostic biosensors. Chem. Soc. Rev. 53 (11), 5394–5427.

Lee, Y.R., Joo, H.K., Jeon, B.H., 2020. The biological role of apurinic/apyrimidinic endonuclease1/redox factor-1 as a therapeutic target for vascular inflammation and as a serologic biomarker. Biomedicines 8 (3), 57.

Li, S.Y., Cheng, Q.X., Liu, J.K., Nie, X.Q., Zhao, G.P., Wang, J., 2018a. CRISPR-Cas12a has both cis-and trans-cleavage activities on single-stranded DNA. Cell Res. 28 (4), 491–493.

Li, S.Y., Cheng, Q.X., Wang, J.M., Li, X.Y., Zhang, Z.L., Gao, S., Cao, R.B., Zhao, G.P., Wang, J., 2018b. CRISPR-Cas12a-assisted nucleic acid detection. Cell Discov 4 (1), 20.

Liu, G., Lin, Q., Jin, S., Gao, C., 2022. The CRISPR-Cas toolbox and gene editing technologies. Mol. Cell 82 (2), 333–347.

Luo, T., Li, J., He, Y., Liu, H., Deng, Z., Long, X., Wan, Q., Ding, J., Gong, Z., Yang, Y., Zhong, S., 2022. Designing a CRISPR/Cas12a-and Au-nanobeacon-based diagnostic biosensor enabling direct, rapid, and sensitive miRNA detection. Anal. Chem. 94 (17), 6566–6573.

Lv, H., Wang, J., Zhang, J., Chen, Y., Yin, L., Jin, D., Gu, D., Zhao, H., Xu, Y., Wang, J., 2021. Definition of CRISPR Cas12a Trans-cleavage units to facilitate CRISPR diagnostics. Front. Microbiol. 12, 766464.

Ma, L., Yin, L., Li, X., Chen, S., Peng, L., Liu, G., Ye, S., Zhang, W., Man, S., 2022. A smartphone-based visual biosensor for CRISPR-Cas powered SARS-CoV-2 diagnostics. Biosens. Bioelectron. 195, 113646.

Pan, J., Deng, F., Liu, Z., Zeng, L., Chen, J., 2023. Construction of molecular logic gates using heavy metal ions as inputs based on catalytic hairpin assembly and CRISPR-Cas12a. Talanta 255, 124210.

Pascut, D., Sukowati, C.H.C., Antoniali, G., Mangiapane, G., Burra, S., Mascaretti, L.G., Buonocore, M.R., Crocè, L.S., Tiribelli, C., Tell, G., 2019. Serum AP-endonuclease 1 (sAPE1) as novel biomarker for hepatocellular carcinoma. Oncotarget 10 (3), 383.

Qiao, Z., Xue, L., Sun, M., Zhang, M., Chen, M., Xu, X., Yang, W., Wang, R., 2023. Highly sensitive detection of Salmonella based on dual-functional HCR-mediated multivalent aptamer and amplification-free Crispr/Cas12a system. Anal. Chim. Acta 1284, 341998.

Shi, H., Doench, J.G., Chi, H., 2023. CRISPR screens for functional interrogation of immunity. Nat. Rev. Immunol. 23 (6), 363–380.

Siti, R.M., Khairunisak, A.R., Abdul Aziz, A., Noordin, R., 2012. Study on controlled size, shape and dispersity of gold nanoparticles (AuNPs) synthesized via seeded-growth technique for immunoassay labeling. Adv. Mater. Res. 364, 504–509.

Song, H., Zeng, J., Lele, S., Lagrange, C.A., Bhakat, K.K., 2021. APE1 and SSRP1 is overexpressed in muscle invasive bladder cancer and associated with poor survival. Heliyon 7 (4), e06756.

Stella, S., Alcón, P., Montoya, G., 2017. Structure of the Cpf1 endonuclease R-loop complex after target DNA cleavage. Nature 546 (7659), 559–563.

Swarts, D.C., Jinek, M., 2019. Mechanistic insights into the cis-and trans-acting DNase activities of Cas12a. Mol. Cell 73 (3), 589–600.

Swarts, D.C., van der Oost, J., Jinek, M., 2017. Structural basis for guide RNA processing and seed-dependent DNA targeting by CRISPR-Cas12a. Mol. Cell 66 (2), 221–233.

Wang, L., Wang, X., Cheng, L., Ding, S., Wang, G., Choo, J., Chen, L., 2021. SERS-based test strips: principles, designs and applications. Biosens. Bioelectron. 189, 113360.

Wang, X., Ding, H., Sun, Y., Ma, Y., Wang, G., Chen, J., Choo, J., Chen, L., 2025. CRISPR/HCR-powered ratiometric fluorescence aptasensor for ochratoxin A detection. Food Chem. 468, 142437.

Wang, X., Zhong, M., Liu, Y., Ma, P., Dang, L., Meng, Q., Wan, W., Ma, X., Liu, J., Yang, G., Yang, Z., Huang, X., Liu, M., 2020. Rapid and sensitive detection of COVID-19 using CRISPR/Cas12a-based detection with naked eye readout, CRISPR/Cas12a-NER. Sci. Bull. (Beijing) 65 (17), 1436–1439.

Wei, X., Li, Y.B., Li, Y., Lin, B.C., Shen, X.M., Cui, R.L., Gu, Y.J., Gao, M., Li, Y.G., Zhang, S., 2017. Prediction of lymph node metastases in gastric cancer by serum APE1 expression. J. Cancer 8 (8), 1492–1497.

Wu, H., Chen, X., Zhang, M., Wang, X., Chen, Y., Qian, C., Wu, J., Xu, J., 2021. Versatile detection with CRISPR/Cas system from applications to challenges. Trends Anal. Chem. 135, 116150.

Xie, J., Li, Y., Kong, J., Li, C., 2019. Apurinic/apyrimidinic endonuclease 1/redox factor-1 could serve as a potential serological biomarker for the diagnosis and prognosis of oral squamous cell carcinoma. J. Oral Maxillofac. Surg. 77 (4), 859–866.

Xu, C., Chen, S., Zhao, J., Luo, X., Zhao, S., 2021. A DNAzyme-mediated target-initiated rolling circle amplification strategy based on a microchip platform for the detection of apurinic/apyrimidinic endonuclease 1 at the single-cell level. Chem. Commun. 57 (84), 11017–11020.

Yi, D., Zhao, J., Li, L., 2021. An enzyme-activatable engineered DNAzyme sensor for cell-selective imaging of metal ions. Angew. Chem. Int. Ed. Engl. 60 (12), 6300–6304.

Zagorovsky, K., Chan, W.C., 2013. A plasmonic DNAzyme strategy for point-of-care genetic detection of infectious pathogens. Angew. Chem. Int. Ed. Engl. 52 (11), 3168–3171.

Zetsche, B., Gootenberg, J.S., Abudayyeh, O.O., Slaymaker, I.M., Makarova, K.S., Essletzbichler, P., Volz, S.E., Joung, J., van der Oost, J., Regev, A., Koonin, E.V., Zhang, F., 2015. Cpf1 is a single RNA-guided endonuclease of a class 2 CRISPR-Cas system. Cell 163 (3), 759–771.

Zhang, S., He, L., Dai, N., Guan, W., Shan, J., Yang, X., Zhong, Z., Qing, Y., Jin, F., Chen, C., Yang, Y., Wang, H., Baugh, L., Tell, G., Wilson, D.M., Li, M., Wang, D., 2016. Serum APE1 as a predictive marker for platinum-based chemotherapy of non-small cell lung cancer patients. Oncotarget 7 (47), 77482.

Zhang, D., Yan, Y., Cheng, X., Yang, T., Li, X., Ding, S., Zhang, X., Cheng, W., 2022. Controlling the trans-cleavage of CRISPR-Cas12a with nicked PAM: universal platform for biosensing. Sens. Actuators B Chem. 353, 131153.

Zhao, W., Brook, M.A., Li, Y., 2008. Design of gold nanoparticle-based colorimetric biosensing assays. Chembiochem 9 (15), 2363–2371.

Zhu, H., Li, C., Gao, C., 2020. Applications of CRISPR-Cas in agriculture and plant biotechnology. Nat. Rev. Mol. Cell Biol. 21 (11), 661–677.